IEEE Access
Multidisciplinary ⋮ Rapid Review ⋮ Open Access Journal

Received 25 July 2022, accepted 23 September 2022, date of publication 30 September 2022, date of current version 12 October 2022.

*Digital Object Identifier 10.1109/ACCESS.2022.3210986*

RESEARCH ARTICLE

# Design of Generalized Sinusoidal Frequency Modulated Pulse Train Waveform to Improve Tracking Performance of High Duty Cycle Sonar Systems

**GEUNHWAN KIM[1], SEOKJIN LEE[2], (Member, IEEE), KYUNGSIK YOON[3], CHANGSOO RYU[4], MINSEUK PARK[5], AND YOUNGMIN CHOO[5], (Member, IEEE)**

[1]Department of Ocean Systems Engineering, Sejong University, Seoul 05006, Republic of Korea
[2]School of Electronics and Electrical Engineering, College of IT Engineering, Kyungpook National University, Daegu 41566, Republic of Korea
[3]Department of IT Convergence Engineering, Gimcheon University, Gamcheon 39528, Republic of Korea
[4]Division of ICT Semiconductor Electronics, Yeungnam University College, Daegu 42415, Republic of Korea
[5]Department of Defense Systems Engineering, Sejong University, Seoul 05006, Republic of Korea

Corresponding author: Youngmin Choo (ychoo@sejong.ac.kr)

This work was supported in part by the Agency for Defense Development (ADD), South Korea, under Grant UD200006DD; and in part by the National Research Foundation of Korea (NRF), South Korea, under Grant 2022R1G1A101094611.

**ABSTRACT** High duty cycle sonar (HDCS) systems have a high potential for improving tracking performance compared to conventional pulsed active sonar systems, but their implementation has been challenging to achieve. This is because conventional waveform design studies for HDCS systems had focused primarily on solving direct blast interference problems caused by continuous transmission and reception of pulse train waveforms. So far, there are no studies for waveform design to improve HDCS tracking performance. In this paper, we proposed a generalized sinusoidal frequency modulated (GSFM) pulse train waveform design scheme to improve HDCS tracking performance. The proposed design scheme utilizes the trade-off relationship between detection performance in a reverberation environment and measurement uncertainty according to the parameter $\rho$ of the GSFM waveform. To accomplish the goal, we developed a framework for pulse train waveform design considering HDCS tracking performance. In the framework, the detection probability and measurement noise covariance matrix of the Kalman filter are calculated based on the designed GSFM pulse train waveform. Therefore, the pulse train waveform design and HDCS tracking performance can be associated. The simulation using the HDCS tracking framework demonstrated that optimal tracking performance was obtained when the parameter $\rho$ was 1.07.

**INDEX TERMS** Generalized sinusoidal frequency modulated waveform, high-duty cycle sonar system, high duty cycle sonar tracking, pulse train waveform design.

## I. INTRODUCTION

Over the past few decades, research on active sonar systems have mainly focused on the pulsed active sonar (PAS) system which transmits a short pulse-type waveform with a long waiting interval when considering its maximum detection range. Due to the long waiting interval, PAS systems suffer from a low target revisit rate (TRR), which leads to a lack of measurements. Consequently, it is difficult to suppress clutter in shallow water and obtain a high tracking performance for long-range moving targets [1], [2], [3].

Recently, the hardware of modern sonar systems have been upgraded enabling a wider dynamic range, and thus solving the problem of saturation when signals with vastly different reception levels are received [3], [4]. From a geometrical perspective, modern sonar technologies show a trend towards the operation of multiple platforms and long-range detection; therefore, research on bistatic systems or multistatic

The associate editor coordinating the review of this manuscript and approving it for publication was Taous Meriem Laleg-Kirati.

sonar systems that are operated with separate transmitters and receivers is being actively conducted [5], [6], [7], [8]. Out of these research trends, a new concept of high duty cycle sonar (HDCS) system is emerging [3], [4], [9], [10], [11], [12], [13], [14], [15], [16], [17], [18], [19], [20], [21], [22], [23], [24].

Unlike the PAS system which transmits a short pulse-type waveform, the HDCS system transmits tens of times longer pulse train waveform which consists of multiple sub-pulses and processes of the received signals using a bank of multiple matched filters in parallel. As each matched filter can obtain independent measurements from the continuously received signal, the HDCS system can obtain tens of times more measurements than the PAS system during the same observation time. These multiple measurements enable the HDCS system to have the potential to remarkably improve the tracking performance [9], [14].

However, achieving high tracking performance of the HDCS system has been challenging because conventional studies of pulse train waveform design had mainly focused on solving the direct blast (DBL) interference problem due to continuous transmission and reception strategy of the HDCS system [15]. If DBL interference is not resolved, the HDCS system cannot operate properly because a small target echo signal is easily masked by a strong DBL interference. To avoid DBL interference problems in HDCS systems, the sub-pulses of the transmit pulse train waveform are designed to possess orthogonality by adjusting the processing strategies. However, these processing strategies inevitably create weaknesses (e.g., trade-off between the bandwidth of the sub-pulses and TRR [9] and independence of measurements [4]). There is a separate study on maintaining the independence of measurements while overlapping the bandwidth of sub-pulses, but which have a drawback of the possibility of limited performance [14], [21].

However, from the tracking point of view, the designed pulse train signal should improve the tracking performance apart from solving the DBL interference problem. There are several studies for associating the waveform design and tracking have been conducted. In radar research, the effect of radar waveform selection and measurement extraction methods on tracking performance has been studied. In the study, tracking performance can be improved by joint consideration of detection and tracking [25]. In the active sonar research, several waveform fusion schemes have been studied and concluded that waveform fusion improves detection and estimation performance [26]. However, to the author's knowledge, the design of pulse train waveforms for improving HDCS tracking performance has not been conducted yet.

In this paper, we propose a generalized sinusoidal frequency modulated (GSFM) pulse train waveform design scheme for improving the tracking performance of the HDCS system by utilizing the trade-off relationship between the detection performance in reverberation environment and the measurement uncertainty. This trade-off relationship was investigated by varying the parameter $\rho$ of the GSFM waveform. To associate the pulse train waveform design and HDCS tracking performance, we developed a framework that simulates the received beam signal in reverberation environments and calculates the probability of detection (relative to detection performance) and the measurement noise covariance matrix (relative to measurement uncertainty) of the Kalman filter for the designed GSFM pulse train waveform.

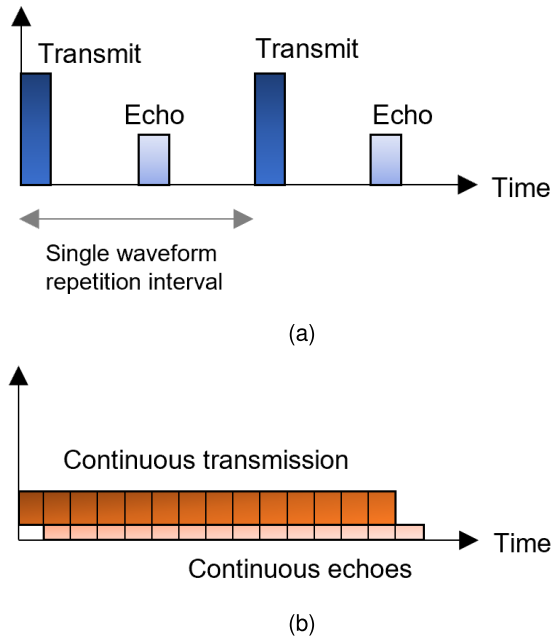


**FIGURE 1.** Comparison of transmission and reception strategies of PAS and HDCS system. In the single waveform repetition interval, PAS system acquires only one measurement but HDCS system can acquire multiple measurements.

The structure of this paper is organized as follows. In Section II, we present the HDCS system and characteristics of GSFM waveform. In Section III, we propose a framework for pulse-train waveform design considering HDCS tracking performance. In Section IV, we conduct a simulation analysis for optimizing $\rho$ of the GSFM pulse train waveform to improve its tracking performance using the proposed framework. In Section V, we conclude the study with a discussion.

## II. PRELIMINARIES

### A. OVERVIEW OF HDCS SYSTEM

Fig. 1 shows a comparison of the transmission and reception strategies of conventional PAS and HDCS systems. Because the HDCS system transmits long pulse train waveforms to increase the TRR, the HDCS system acquires tens of times more measurements per single waveform repetition interval than the conventional PAS system. Therefore, the HDCS system has more potential to achieve higher tracking performance than the PAS system [9], [11].

The signal model of pulse train waveform of the HDCS system consists of sub-pulses of length $T_{sub}$ as follows [21], [27]:

$$s(t) = \sum_{n=1}^{N} s_n(t - (n-1)T_{sub}), \tag{1}$$

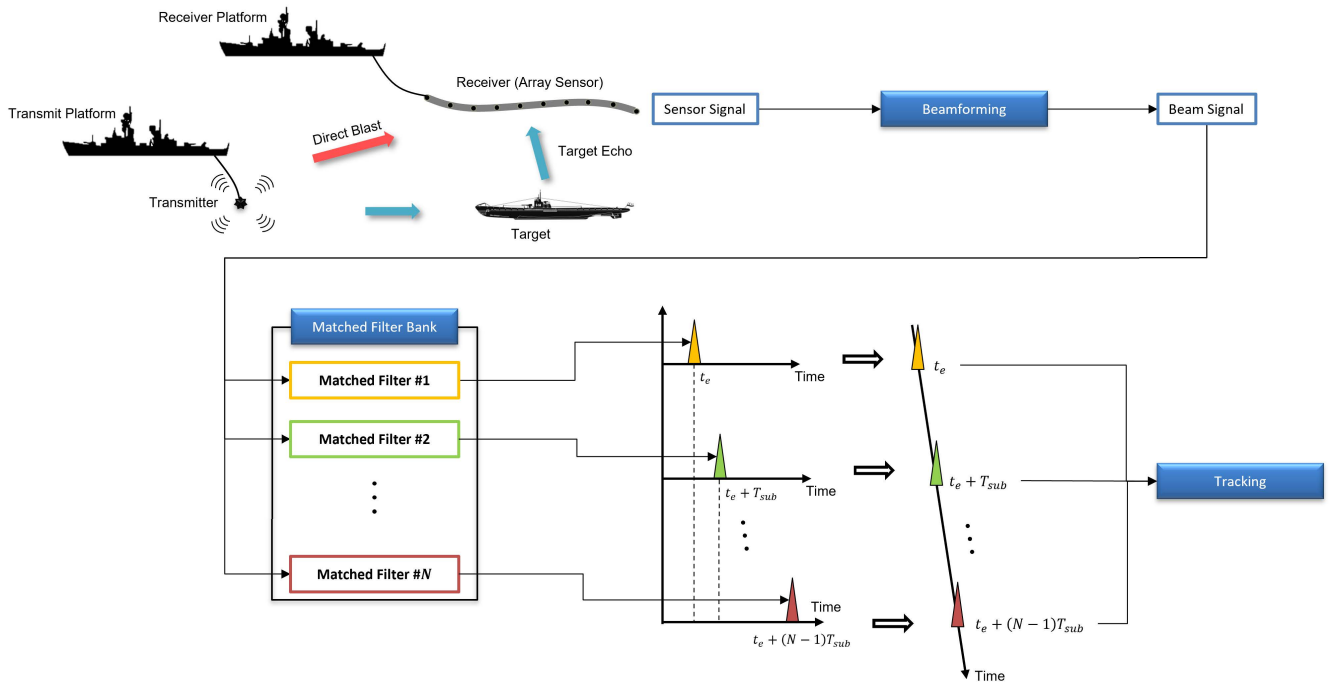


**FIGURE 2.** Signal processing scheme of the HDCS system. Target echo signal is received along with the DBL interference and beamforming is applied. After beamforming, beam signal is applied to the matched filter bank which consists of multiple parallel matched filters to detect target. Therefore, HDCS system can acquire $N$ measurements with interval $T_{sub}$. All of $N$ measurements achieved from detection process are used in the tracking process.

where $N$ is the number of sub-pulses, $T_{sub}$ is the length of each sub-pulse, and $s_n(t)$ is the $n^{th}$ sub-pulse, which we express as follows:

$$s_n(t) = w(t)e^{j\varphi_n(t)}e^{j2\pi(f_c+\Delta f_n)t}, \tag{2}$$

where $w(t)$ is the window function, $f_c$ is the center frequency of pulse train waveform, $\Delta f_n$ is the hopping frequency of the $n^{th}$ sub-pulse, and $\varphi_n(t)$ is the phase modulation function which determine the characteristics of $n^{th}$ sub-pulse. The instantaneous frequency (IF) function of $n^{th}$ sub-pulse $f_n(t)$ is given by

$$f_n(t) = \left(\frac{1}{2\pi}\right)\frac{\partial\varphi_n(t)}{\partial t}. \tag{3}$$

Fig. 2 shows the signal processing scheme of the HDCS system when the pulse train waveform consists of $N$ sub-pulses of length $T_{sub}$. The HDCS system uses a bank of parallel matched filters to process each sub-pulse of the pulse-train waveform. Each matched filter in the bank is designed to handle a corresponding sub-pulse. If the arrival time of the target echo owing to the first sub-pulse is $\tau_e$, the arrival time of the target echo owing to $n^{th}$ sub-pulse is $\tau_e + (n-1)T_{sub}$. Consequently, the total number of measurements is $N$ and its interval is $T_{sub}$. After the detection process, all $N$ measurements were used in the tracking process. $N$ times more measurements give the tracking process a significant advantage in improving tracking performance [10], [13], [16].

Theoretically, multiple measurements can be obtained by using the HDCS system, but many practical problems are faced in obtaining high tracking performance [3], [10]. Among these, DBL interference is the most problematic [15]. To alleviate the DBL interference, orthogonality is prioritized when designing a pulse train waveform. For this reason, it was difficult to consider the detection performance in the reverberation environment and measurement uncertainty, which plays an important role in conventional active sonar research, in the previous studies on HDCS pulse-train design [9], [14], [21].

### B. GSFM WAVEFORM AND ITS CHARACTERISTICS

The GSFM waveform introduced in [14] is a waveform originally developed to modify a sinusoidal frequency modulation (SFM) waveform to obtain thumbtack-ambiguity with a good range-Doppler resolution at the same time. Because the GSFM waveform can produce an orthogonal waveform by altering the parameters, it was used to design pulse train waveforms for HDCS systems in previous studies [14], [28]. In this study, however, we would like to observe the trade-off characteristic of the GSFM waveform according to its parameter $\rho$ (parameter $\rho$ will be covered in (4)). In this subsection, the signal model of the GSFM waveform is introduced, followed by the trade-off relationship according to parameter $\rho$.

The phase modulation function of the GSFM waveform can be expreseed as follows:

$$\varphi(t;\alpha,\rho) = \frac{\beta}{t^{(\rho-1)}}\sin\left(\frac{2\pi\alpha\rho}{\rho}\right). \tag{4}$$

The IF function of the GSFM waveform can be calculated using (3) as follows:

$$f(t;\alpha,\rho)=\beta\alpha\left[\cos\left(\frac{2\pi\alpha t^{\rho}}{\rho}\right)-\left(\frac{\rho-1}{\rho}\right)\times\operatorname{sinc}\left(\frac{2\pi\alpha t^{\rho}}{\rho}\right)\right], \quad (5)$$

where $\beta$ represents the modulation index as $\beta = B/2\alpha$ and $\alpha$ is a frequency modulation term that determines the number of cycles included in the IF function of the GSFM pulse. $B$ is the pulse bandwidth. The cycle was calculated as $C = \alpha T^{\rho}/\rho$, where $\rho$ ($\geq 1$) is a dimensionless parameter that controls the shape of the IF function of the GSFM waveform.

In [27], it was mentioned that the trade-off relationship between the detection performance in reverberation environment and measurement uncertainty according to the $\rho$ in the low range where the value approaches one. The reason for this trade-off is as follows: As $\rho$ is closer to 1, the IF function is designed to be that of the SFM waveform, which has superior detection performance in reverberation. As $\rho$ is further away from one, conversely, the IF function is designed to be that of the time-voltage characteristics of LFM waveform, which has a high pulse compression gain (see Appendix A for a detailed review of the trade-off relationship of the GSFM waveform).

Although the trade-off relationship of GSFM waveform was known, it was regarded as noncommittal because neither performance was satisfactory and hence did not receive much attention. In this study, however, we want to utilize this property to improve the tracking performance of HDCS system. In other words, we claim that a GSFM pulse train waveform with superior tracking performance can be designed using the trade-off between detection performance and measurement uncertainty. Before proceeding further, however, a specific methodology is required that reflects the characteristics of the GSFM pulse train waveform designed in the HDCS tracking process.

## III. FRAMEWORK DEVELOPMENT FOR PULSE TRAIN WAVEFORM DESIGN CONSIDERING TRACKING PERFORMANCE

In this section, we propose the framework for pulse train waveform design considering HDCS tracking performance. A similar concept was studied in radar waveform selection [25] and PAS waveform fusion [26]; however, these methodologies are not suitable for HDCS tracking assessment. To the best of our knowledge, no studies have considered tracking performance when designing pulse train waveforms for HDCS systems.

Fig. 3 shows the scheme of the proposed framework for pulse train waveform design considering the tracking performance. In the proposed framework, a Kalman filter is used as the tracking algorithm [29]. The difference of the Kalman filter used here from an ordinary Kalman filter is that the measurement noise covariance matrix $\mathbf{R}$ (here, it means measurement uncertainty) and detection probability $P_D$ (here, it means detection performance) are computed from outside the Kalman filter. Looking back along the arrow, it can be seen that the two values were calculated from the designed pulse train waveform. Therefore, it is able to implement our goal of associating waveform design and tracking performance. Now, each part of the framework is explained individually.

### A. WAVEFORM GENERATION

In this part, the time signal of $N$ sub-pulses of GSFM pulse train waveform are generated using (1) to (5). Each GSFM sub-pulse was designed to have the same $\alpha$ and $\rho$. The generated time signals of the sub-pulses are utilized in the following process.

### B. SIGNAL SYNTHESIS

In this part, the received beam signal is synthesized by simulating reverberation environments of HDCS system. The received beam signal of reverberation can be expressed as [30] and [28]

$$r(t)=\sum_{i}\sum_{n=1}^{N}a_i s_n(\eta_i(t-\tau_i)), \quad (6)$$

where $a_i$ is the scattered amplitude of $i^{th}$ scatterer, $\eta_i$ is Doppler scaling factor of $i^{th}$ scatterer, and $\tau_i$ is time delay of $i^{th}$ scatterer. The reverberation signal is generated by summing the signals of all $N$ sub-pulses, considering the effect of the continuous transmission and reception scheme of the HDCS system.

The received beam signal of target echo due to $n^{th}$ sub-pulse can be expressed as follows:

$$e_n(t) = a_e s_n(\eta_e(t-\tau_e)), \quad (7)$$

where $a_e$ is amplitude of target echo, $\eta_e$ is Doppler scaling factor of target echo, and $\tau_e$ is time delay of target echo. Note that the received beam signal of the target echo is generated individually for every sub-pulse.

General noise signal except reverberation was modeled as additive white Gaussian noise (AWGN) $\nu(t)$ with zero-mean and variance of $\sigma_N^2$.

Now, we can generate signals of null hypothesis (absent of target echo) and alternative hypothesis (present of target echo) by combining $r(t)$, $e_n(t)$, and $\nu(t)$ as follows [31], [32]:

$$\begin{cases}\mathcal{H}_0 : x_0(t) = r(t)+\nu(t)\\ \mathcal{H}_{1,n} : x_{1,n}(t) = e_n(t)+r(t)+\nu(t)\end{cases} \quad (8)$$

where $\mathcal{H}_0$ is the null hypothesis, ($x_0(t)$ is signal of absent of target echo) and $\mathcal{H}_{1,n}$ is the alternative hypothesis of $n^{th}$ sub-pulse, ($x_{1,n}(t)$ is signal of present target echo with $n^{th}$ sub-pulse). Note that the alternative hypothesis is generated individually for every sub-pulse, and these are depicted as switches in Fig. 3.

The power of each signal could be calculated as follows: once $\sigma_N^2$ is set, the power of target signal can be set by comparing with AWGN noise, signal-to-noise ratio (SNR),

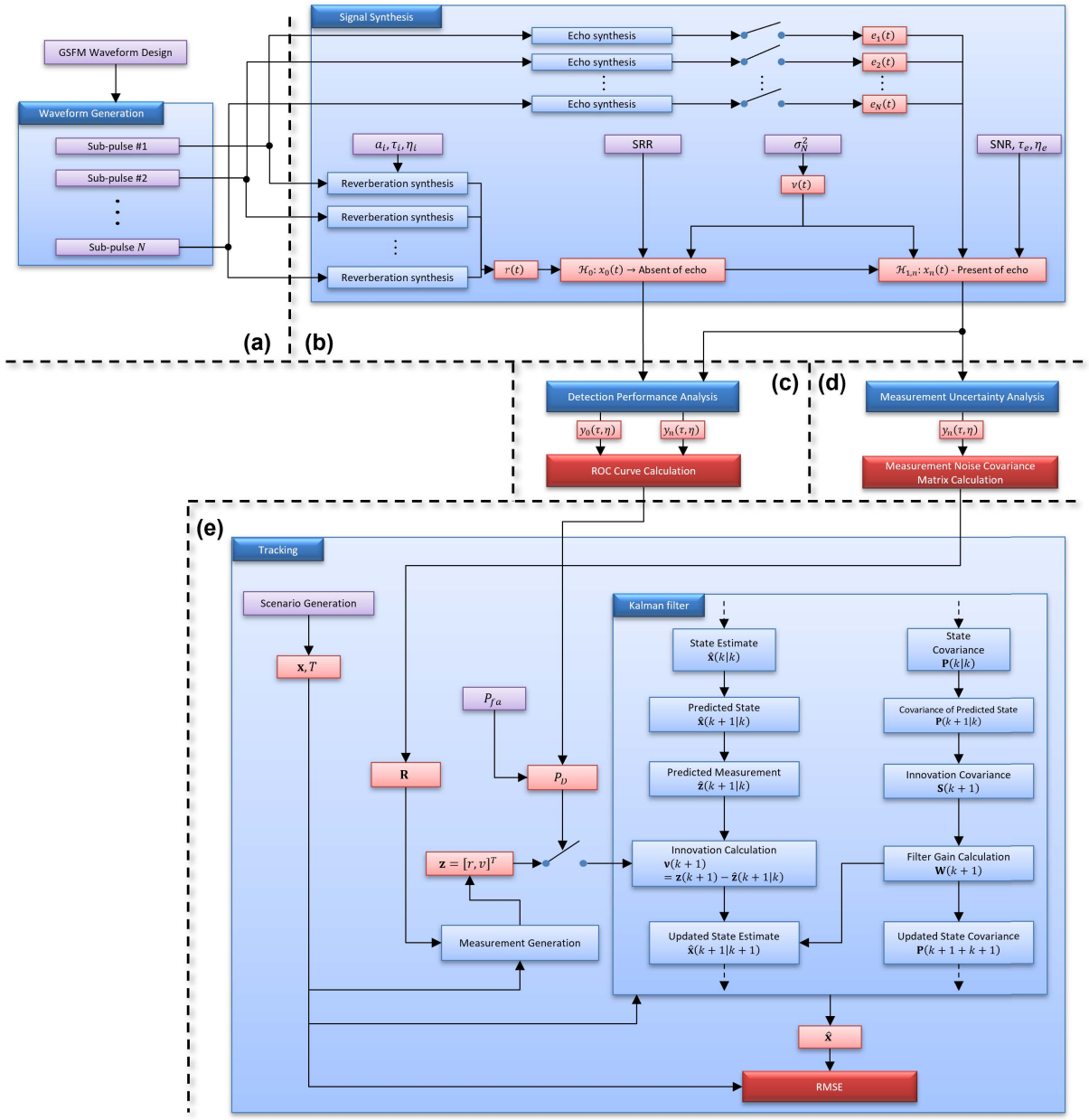


**FIGURE 3.** Proposed framework for pulse train waveform design considering tracking performance. In the proposed framework, detection performance and measurement uncertainty of the designed pulse train waveform is reflected in the tracking process as the probability of detection $P_D$ and measurement noise covariance matrix **R** of the Kalman filter, respectively. (a) Waveform generation part. In this part, the time signal of the pulse train waveform is generated. (b) Signal synthesis. In this part, the received beam signal is synthesized by simulating practical operation environments of the HDCS system. (c) Detection performance analysis. In this part, the ROC curve is calculated to assess the detection performance of the designed pulse train waveform. (d) Measurement uncertainty analysis. In this part, the sample measurement noise covariance matrix is calculated to assess the measurement uncertainty of the designed pulse train waveform. (e) Tracking. In this part, a tracking simulation is conducted using the modified Kalman filter algorithm to reflect the detection performance and measurement uncertainty of the designed pulse train waveform.

then reverberation power can be set by comparing with the power of target signal, signal-to-reverberation ratio (SRR).

### C. DETECTION PERFORMANCE ANALYSIS

This part evaluates the detection performance of the designed pulse train waveform in reverberation environments. Detection performance was assessed using the receiver operating characteristic (ROC) curve. ROC curve can be calculated from the matched filter (MF) results of the Monte Carlo simulation (multiple realizations of the synthesized signal of the two hypotheses). The MF results for each hypothesis are expressed as follows.

$$\begin{cases} \mathcal{H}_{0,n} : y_{0,n}(\tau, \eta) = \int x_0(t)\, s_n(\eta(t-\tau))dt \\ \mathcal{H}_{1,n} : y_{1,n}(\tau, \eta) = \int x_{1,n}(t; \tau_e, \eta_e) s_n(\eta(t-\tau))dt \end{cases} \tag{9}$$

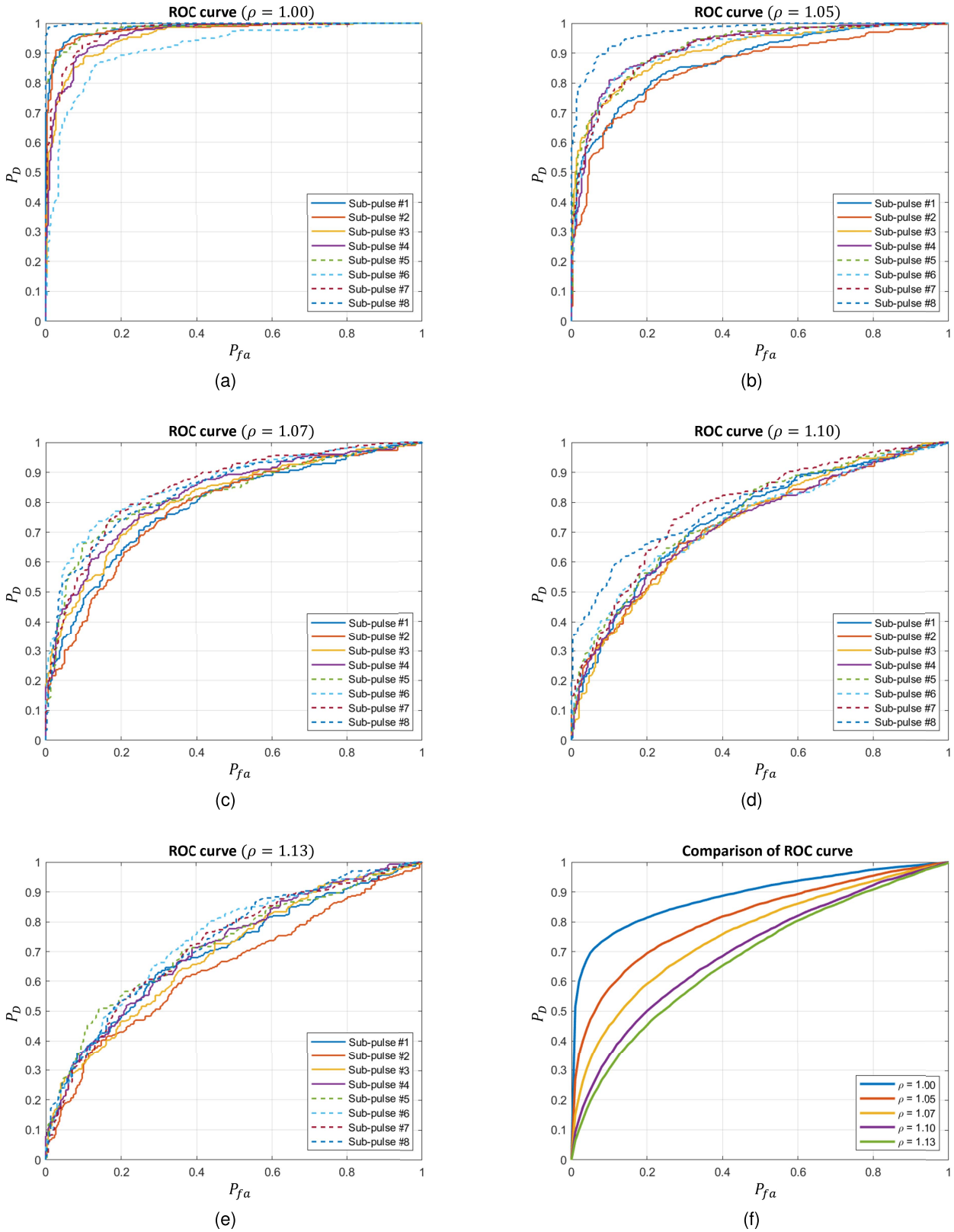


**FIGURE 4.** Calculated ROC curve of the GSFM pulse train waveform using the proposed framework with $\rho$ of (a) 1.00, (b) 1.05, (c) 1.07, (d) 1.10, and (e) 1.13. In (f), the average of the ROC curves of each case of $\rho$ are presented. As $\rho$ increases, it can be seen that the detection performance is decreased.

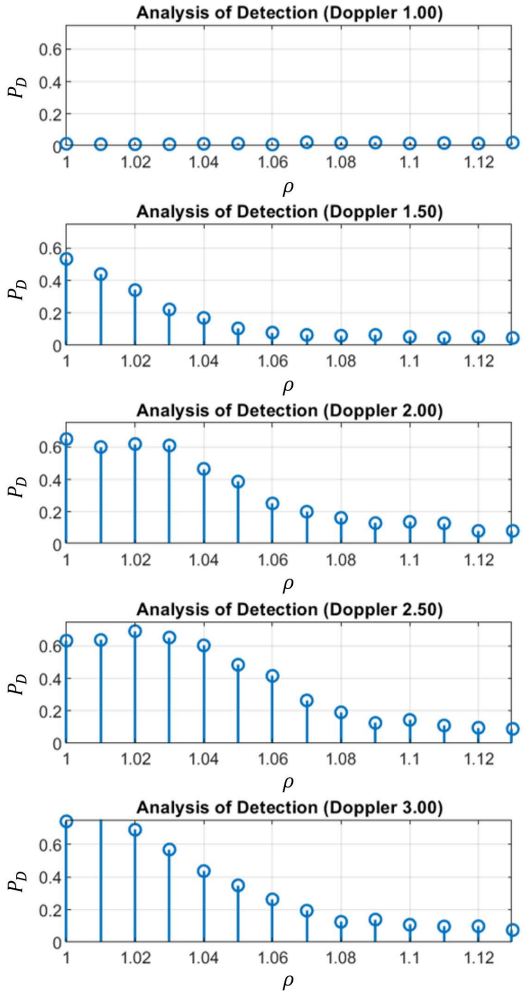


**FIGURE 5.** Selected probability of detection $P_D$ at probability of false alarm $P_{fa}$ is 0.01 from ROC curve. Except for cases where the Doppler is too low to detect (Doppler value of 1.00 m/s), as $\rho$ increases, $P_D$ tends to decrease.

where $\tau$ is time delay, $\eta$ is Doppler scaling factor, and $y_{0,n}(\tau)$ and $y_{1,n}(\tau)$ are MF results of null hypothesis and alternative hypothesis when $n^{th}$ sub-pulse is used as a replica, respectively. Note that $x_{1,n}(t;\tau_e,\eta_e)$ means that the target echo has a time delay of $\tau_e$ and a Doppler of $\eta_e$. Although time delay does not affect detection performance, the Doppler has a severe effect on detection performance. In other words, the characteristics of the ROC curve depending on the Doppler of target echo. Therefore, the ROC curve should be calculated individually for every sub-pulse and Doppler signal.

The probability of detection $P_D$ and the probability of false alarm $P_{fa}$ of ROC curve can be calculated numerically through calculating with varying threshold and can be depicted as follows [33], [34]:

$$P_D = \frac{N_{TP}}{N_{Pos}}, \tag{10}$$

$$P_{fa} = \frac{N_{FP}}{N_{Neg}}. \tag{11}$$

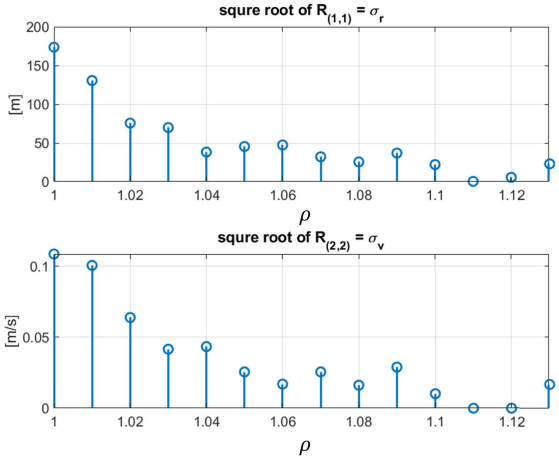


**FIGURE 6.** First and second diagonal elements which mean range measurement uncertainty and the velocity measurement uncertainty of calculated sample measurement noise covariance matrix R, respectively. Both measurement uncertainty is improved as $\rho$ increases.

where $N_{Pos}$ is the number of positives (detection cell containing the target echo), $N_{Neg}$ is number of negatives (detection cell with no target echo), $N_{TP}$ is number of true positives (detection cell greater than threshold when it containing the target echo), and $N_{FP}$ is number of false positives (any detection cell which is greater than threshold).

### D. MEASUREMENT UNCERTAINTY ANALYSIS

This part evaluates the measurement uncertainty of the designed pulse train waveform by calculating the measurement noise covariance matrix $\mathbf{R}_n$ for every $n^{th}$ sub-pulse. $\mathbf{R}_n$ was obtained by calculating the sample covariance matrix of the error vector $\mathbf{w}_n$ from the Monte Carlo simulation of MF. Error vector $\mathbf{w}_n$ can be expressed as follows:

$$\mathbf{w}_n = \mathbf{z}_n^{true} - \mathbf{z}_n^{est}, \tag{12}$$

where $\mathbf{z}_n^{true}$ is true measurement vector and $\mathbf{z}_n^{est}$ is estimated measurement vector. $\mathbf{z}_n^{true}$ can be expressed as

$$\mathbf{z}_n^{true} = \begin{bmatrix} \tau_e \\ \eta_e \end{bmatrix}, \tag{13}$$

where $\tau_e$ and $\eta_e$ is time delay and Doppler of target echo, respectively. $\mathbf{z}_n^{est}$ can be expressed as

$$\mathbf{z}_n^{est} = \text{argmax}_{\tau,\eta} \left| y_{1,n}(\tau,\eta) \right| = \begin{bmatrix} \hat{\tau} \\ \hat{\eta} \end{bmatrix}, \tag{14}$$

where $y_{1,n}(\tau,\eta)$ is MF results of alternative hypothesis of $n^{th}$ sub-pulse in (9). $\hat{\tau}$ and $\hat{\eta}$ are the estimated time delay and Doppler scaling factor, respectively. $\mathbf{z}_n^{est}$ is estimated from the peak of the MF output. This is possible under the assumption that only one target echo exists in the region of interest.

Since it is preferable to express the state of the measured value in terms of distance and velocity in the Kalman filter, the time delay $\tau$ and Doppler scaling factor $\eta$ are converted

into distance and velocity using the following relationship:

$$r = c\tau/2, \tag{15}$$
$$v = c(\eta - 1)/2. \tag{16}$$

Therefore, (13) and (14) are converted as follows:

$$\mathbf{z}_n^{true} = \begin{bmatrix} r_e \\ v_e \end{bmatrix}, \tag{17}$$
$$\hat{\mathbf{z}}_n^{est} = \begin{bmatrix} \hat{r} \\ \hat{v} \end{bmatrix}. \tag{18}$$

The sample measurement noise covariance matrix of $n^{th}$ sub-pulse can be calculated as follows:

$$\mathbf{R}_n = \frac{1}{M}\sum_{i=1}^{M} \mathbf{w}_n^{(i)} \mathbf{w}_i^{(i)T}, \tag{19}$$

where superscript $(i)$ means $i^{th}$ sample of Monte-Carlo simulation and $M$ is the number of Monte-Carlo trial.

### E. TRACKING

This part is essential for the proposed framework because the system performance (tracking performance) obtained from this part gives the performance metric of the designed pulse train waveform for the HDCS system. The main tracking algorithm is implemented by the Kalman filter [29]; however, its structure differs from that of the ordinary Kalman filter in the measurement update process.

State equation of the Kalman filter can be expressed as follows:

$$\mathbf{x}(k+1) = \mathbf{F}\mathbf{x}(k) + \mathbf{v}(k), \tag{20}$$

where $\mathbf{x}(k) = [r, v]^T$ is a state vector, $r$ is range, $v$ is velocity, $\mathbf{F}$ is transition matrix, and $\mathbf{v}(k)$ is process noise vector with covariance matrix $\mathbf{Q} = E\left[\mathbf{v}(k)\,\mathbf{v}^T(k)\right]$ and zero-mean. The measurement equation is as follows:

$$\mathbf{z}(k) = \mathbf{H}\mathbf{x}(k) + \mathbf{w}(k), \tag{21}$$

where $\mathbf{z}(k)$ is measurement vector, $\mathbf{H}$ is measurement matrix, and $\mathbf{w}(k)$ is measurement noise vector with covariance matrix $\mathbf{R} = E\left[\mathbf{w}(k)\,\mathbf{w}^T(k)\right]$ and zero-mean. Also, we have

$$\mathbf{F} = \begin{bmatrix} 1 & \Delta T \\ 0 & 1 \end{bmatrix}, \tag{22}$$
$$\mathbf{H} = \begin{bmatrix} 1 & 0 \\ 0 & 1 \end{bmatrix}, \tag{23}$$
$$\mathbf{Q} = \begin{bmatrix} \Delta T^4/4 & \Delta T^3/2 \\ \Delta T^3/2 & \Delta T^2 \end{bmatrix}, \tag{24}$$

where $\Delta T$ is measurement sampling interval of Kalman filter and $c$ is speed of sound.

From (20) and (21), Kalman filter algorithm can be derived [29], however, unlike ordinary Kalman filter, detection performance and measurement uncertainty of designed pulse train waveform are reflected as probability of detection $P_D$ (as explained in Sec. III-C) and measurement noise covariance matrix $\mathbf{R}$ (as explained in Sec. III-D), respectively. These values vary depending on the sub-pulse and target Doppler, and whenever the Kalman filter is updated according to the tracking scenario, pre-calculated values suitable for the scenario are selected and used.

Prediction process of the Kalman filter algorithm can be expressed as follows:

$$\hat{\mathbf{x}}(k+1|k) = \mathbf{F}\hat{\mathbf{x}}(k|k), \tag{25}$$
$$\mathbf{P}(k+1|k) = \mathbf{F}\mathbf{P}(k+1|k)\mathbf{P}^T + \mathbf{Q}, \tag{26}$$

where $\hat{\mathbf{x}}(k+1|k)$ is predicted state vector and $\mathbf{P}(k+1|k)$ is noise covariance matrix of the predicted state vector.

After the prediction process, the predicted state vector in (25) will be updated using the measurement vector $\mathbf{z}(k+1)$ obtained at this update interval. The update process is performed stochastically according to $P_D$ which is selected at a specific $P_{fa}$ from the calculated ROC curve. The stochastically measurement update can be implemented by realizing a random variable $u$ that follows a uniform distribution with boundaries of 0 to 1.

The update process of the Kalman filter algorithm can be expressed as follows:

$$\hat{\mathbf{x}}(k+1|k+1) = \hat{\mathbf{x}}(k+1|k) + \mathbf{W}(k+1)\boldsymbol{\nu}(k+1), \tag{27}$$
$$\mathbf{P}(k+1|k+1) = [\mathbf{I} - \mathbf{W}(k+1)\mathbf{H}\mathbf{P}(k+1|k)]. \tag{28}$$

where $\hat{\mathbf{x}}(k+1|k+1)$ is the updated state vector, $\mathbf{I}$ is identity matrix, and $\boldsymbol{\nu}(k+1)$ is innovation vector which can be expressed as follows:

$$\boldsymbol{\nu}(k+1) = \mathbf{z}(k+1) - \hat{\mathbf{z}}(k+1|k), \tag{29}$$
$$\hat{\mathbf{z}}(k+1|k) = \mathbf{H}\hat{\mathbf{x}}(k+1|k). \tag{30}$$

where $\hat{\mathbf{z}}(k+1|k)$ is the predicted measurement vector and $\mathbf{z}(k+1)$ is the measurement vector which is generated by two-dimensional Gaussian distribution with true mean according to the scenario and measurement noise covariance matrix $\mathbf{R}$ according to sub-pulse in (19). $\mathbf{W}(k+1)$ is Kalman gain, which can be expressed as

$$\mathbf{W}(k+1) = \mathbf{P}(k+1|k)\mathbf{H}^T\mathbf{S}^{-1}(k+1). \tag{31}$$
$$\mathbf{S}(k+1) = \mathbf{H}\mathbf{P}(k+1|k)\mathbf{H}^T + \mathbf{R}, \tag{32}$$

where $\mathbf{S}(k+1)$ is noise covariance matrix of innovation vector.

After the Monte-Carlo simulation of the tracking process, root mean square error (RMSE) is calculated for performance evaluation of HDCS system and defined as follows:

$$\mathrm{RMSE}^{pos}(k) = \sqrt{\sum_{i=1}^{M} \frac{\left(r_i(k) - r_i^{est}(k)\right)^2}{M}}, \tag{33}$$
$$\mathrm{RMSE}^{vel}(k) = \sqrt{\sum_{i=1}^{M} \frac{\left(v_i(k) - v_i^{est}(k)\right)^2}{M}}, \tag{34}$$

where $r_i(k)$ is true position, which is the first element of the true state vector $\mathbf{x}_i(k)$, $r_i^{est}(k)$ is estimated position which is the first element of the estimated state vector $\mathbf{x}_i^{est}(k)$, $v_i(k)$ is

**TABLE 1. Summary of the Kalman filter algorithm in the proposed framework.**

1. Initial:
   a) Set F using (22)
   b) Set H using (23)
   c) Set Q using (24)

**while** $t \leq$ Duration
   2. Parameters:
      a) Set $P_D$ using Sec. III-C
      b) Set $\mathbf{R}$ using Sec. III-D

   3. Prediction:
      a) Predict the state vector using (25)
      b) Calculate the noise covariance matrix of the predicted state vector using (26)

   **if** $u \geq P_D$
      4. Update:
         a) Transform the predicted state vector to predicted measurement vector using (30)
         b) Calculate the innovation vector using (29)
         c) Update the state vector using (27), (32), and (31)
         d) Calculate the noise covariance matrix of the updated state vector using (28)
         e) Estimated state vector: $\mathbf{x}^{est}(k) = \hat{\mathbf{x}}(k+1|k+1)$
   **else**
         f) Estimated state vector: $\mathbf{x}^{est}(k) = \mathbf{x}(k+1|k)$

true velocity which is the second element of the true state vector $\mathbf{x}_i(k)$, and $r_i^{est}(k)$ is estimated velocity which is the second element of the estimated state vector $\mathbf{x}_i^{est}(k)$ at $k^{th}$ time frame in $i^{th}$ Monte-Carlo trial. $M$ denotes the number of Monte Carlo trials. We can use the average value of the RMSE as a metric to compare the superior relationships for different pulse train waveforms. Table 1 summarizes the Kalman filtering algorithm used in the proposed framework.

## IV. SIMULATION

In this section, we attempt to optimize the $\rho$ parameter of GSFM pulse train waveform and analyze the results through the simulation. In the simulation, the center frequency $f_c$, system bandwidth $B_{sys}$ of GSFM pulse train waveform, and length of each sub-pulse $T_{sub}$ are set to 3 kHz, 1 kHz, and 2 s, respectively. The number of sub-pulses $N$ is set to eight; therefore, the total length of GSFM pulse train waveform is 16 s. However, we set the waveform repetition interval to 20 s; therefore, a rest time of 4 s existed. Each frequency band of the sub-pulses is set to separate; consequently, the bandwidth of the sub-pulse $B_{sub}$ is set to 125 Hz. The purpose of the separated-band design is to minimize the effect of DBL interference and, consequently, to focus on the research on tracking performance according to $\rho$. The parameter $C$ of GSFM waveform was set to 40. This value was designed considering the null position in the Doppler axis of SFM waveform.

Simulation parameters of signal synthesis parts are set as follows: The number of scatterers is set to 300. The time delay $\tau_i$ of scatterers is set to a uniform distribution, the attenuation factor $a_i$ is set to a normal distribution with a mean of 1 and a standard deviation of 0.3, and the Doppler factor $\eta_i$ is set to a normal distribution with a mean of 0 and a standard deviation of 3 m/s. The powers of the target and reverberation signals were synthesized at -3 dB and 10 dB, respectively, based on the power of AWGN ($\sigma_N^2$). Consequently, the SRR was set to -13 dB. The target Doppler value is set to 1 m/s to 3 m/s with 0.5 m/s intervals. The number of Monte Carlo trials for ROC curve and $\mathbf{R}$ is set to 100. The false-alarm rate $P_{fa}$ for calculating the detection probability $P_D$ was set to 0.1. This is a large value in a general sonar system; however, when a lower $P_{fa}$ is applied, the number of Monte Carlo trials increases rapidly. Because the result would not change even if $P_{fa}$ was set to a low value and the purpose of this study was to compare the system performance of the pulse train waveform, we set $P_{fa}$ to 0.1.

In Fig. 4 (a) to (e), show the ROC curve of eight sub-pulses of GSFM pulse train waveform with $\rho$ of 1.00, 1.05, 1.07, 1.10, and 1.13, respectively, at Doppler of 2.0 m/s. From these figures, we can interpret that the GSFM pulse train waveform with low $\rho$ shows superior detection performance, and it decreases as $\rho$ increases. Fig. 4 (f) shows a comparison of ROC curves with different $\rho$ values, which accumulates the effect of all the Doppler cases. This figure clearly shows that the detection performance of the GSFM pulse-train waveform depends on $\rho$, as expected from Fig. 4 (a)-(e).

In Fig. 5 shows the probability of detection according to the parameter $\rho$ at Doppler velocities of 1.0, 1.5, 2.0, 2.5, 3.0 m/s, respectively, at $P_{fa}$ of 0.01. The case of the Doppler value of 1.00 m/s in Fig. 5 (a) shows a low detection probability close to zero for all $\rho$ values because 1.0 m/s is too low and is mostly masked by the reverberation spectrum. However, at Doppler velocities greater than 1.5 m/s, it can be seen that the detection probability is high at low $\rho$ and decreases as $\rho$ increases. This is because, as described above, as $\rho$ increases, it exhibits more properties of the GSFM waveform, and the detection performance in reverberation deteriorates. At 1.5 m/s Doppler, the difference in detection probability between $\rho$ of 1.00 and 1.13 is 0.487, but as the Doppler value increases, the difference widens to more than 0.7. This phenomenon occurs because 3.0 m/s is closer to the null position of the Q-function of GSFM than Doppler of 1.5 m/s.

Fig. 6 shows the square root of the diagonal terms of the calculated measurement noise covariance matrix $\mathbf{R}$ according to $\rho$ (which averages the value of all calculated measurement noise covariance matrices of each sub-pulse and Doppler case). Therefore, their values are the standard deviations of the range and velocity estimations, respectively. In the first figure, as $\rho$ increases, it can be seen that the range uncertainty decreases as it approaches the GSFM waveform. The second figure confirms that the uncertainty of the velocity estimation tends to decrease as $\rho$ increases. From Fig. 5 and Fig. 6, we can observe the range uncertainty and detection perfor-

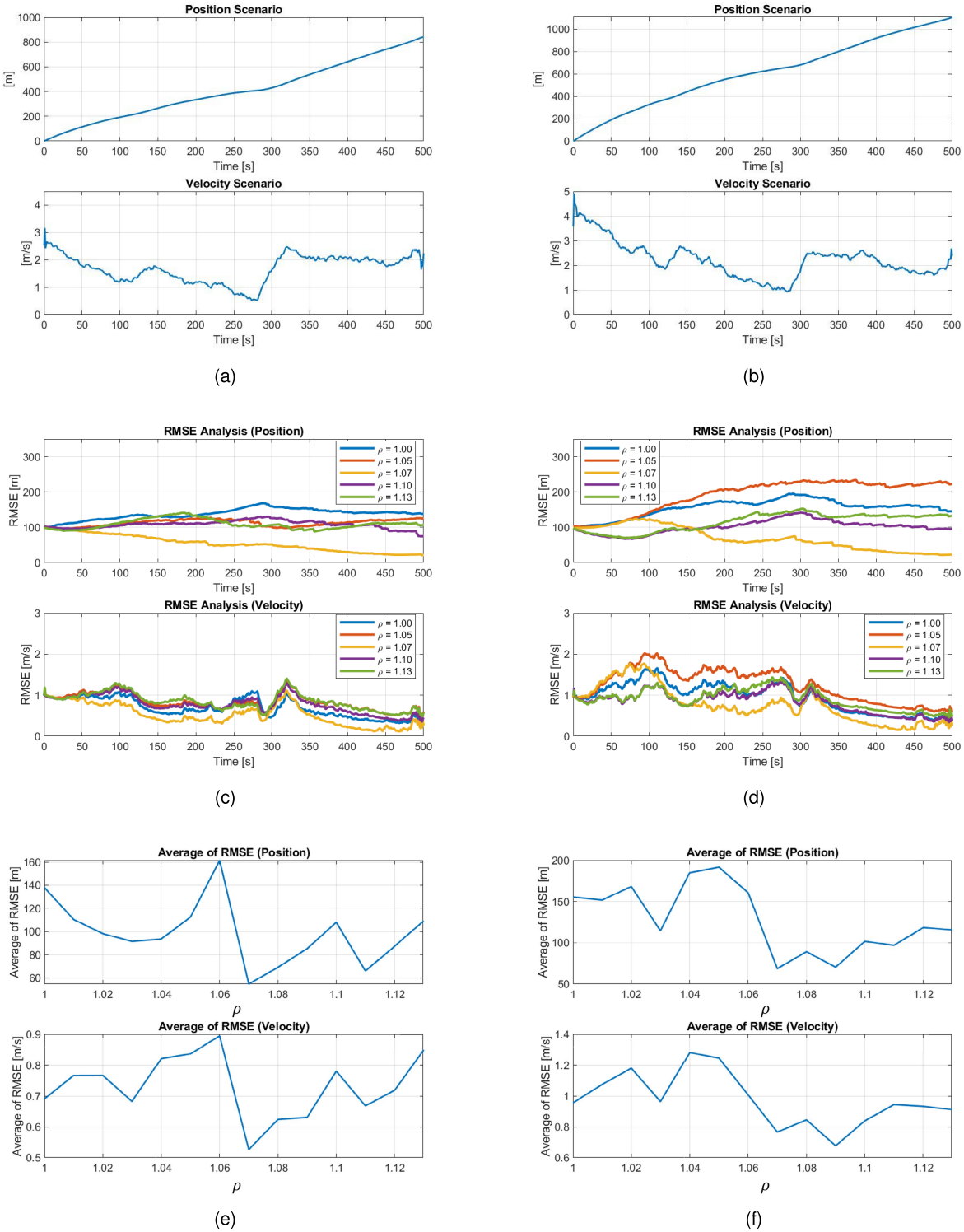


**FIGURE 7.** Simulation of HDCS tracking process using the proposed frameworks. (a) and (b) present two tracking scenarios with different maneuvering target. (c) and (d) present the RMSE of tracking process of two tracking scenarios, respectively. In both scenarios, when $\rho$ is 1.07, it can be seen that the RMSE is lower than the other $\rho$ in the overall duration. (e) and (f) present the average RMSE of tracking process according to various $\rho$. The first tracking scenario shows a low average RMSE when $\rho$ is 1.07 and the second tracking scenario shows a low average RMSE when $\rho$ is 1.07 and 1.09. Therefore, it was confirmed that the tracking performance of the GSFM pulse train waveform is optimized when $\rho$ is 1.07 using the proposed framework. In other words, a GSFM pulse train waveform with an $\rho$ of 1.07 provides a good compromise between sensing performance and measurement uncertainty.

mance in the reverberation trade-off relationship of GSFM waveform according to parameter $\rho$.

Since the detection probability and $\mathbf{R}$ were calculated, the tracking process could be performed. The sampling interval of Kalman filter $\Delta T$ was set to 2 s, considering the length of the sub-pulse. Parameter $q$ of the process covariance matrix $\mathbf{Q}$ was set to 0.1. The number of Monte Carlo trials for the tracking analysis was set to 1000. The initial position was set to be random with a standard deviation of 100 m and a zero-mean normal distribution.

In this study, two tracking scenarios were set as shown in Fig. 7 (a) and (b) to evenly analyze the results for different maneuvering scenario. The total duration was set to 500 s and only one-dimensional maneuvers of the target were considered. In the scenario of Fig. 7 (a), the speed of the target varies between 0.6 m/s and 3.0 m/s, and the speed change is set to change irregularly as in the real world. In the scenario of Fig. 7 (b), the speed of the target varies between 1.0 m/s and 5.0 m/s, and the speed change is also changed irregularly as in the real world.

In Fig. 7 (c) shows RMSE results for the tracking scenario in Fig. 7 (a) for $\rho$ values of 1.00, 1.05, 1.07, 1.10, and 1.13, respectively. In the position tracking analysis, in the case of $\rho$ except 1.07, RMSE fluctuates near 100 m, but RMSE of $\rho$ of the 1.07 case shows a steady decrease. The velocity tracking analysis of cases where $\rho$ is 1.07 shows the lowest result among the five cases. Fig. 7 (d) shows RMSE results of tracking scenario in Fig. 7 (b) for $\rho$ values of 1.00, 1.05, 1.07, 1.10, and 1.13, respectively. Although the detailed trends are different, it can be seen that similar to the result of the first scenario in Fig. 7 (c), when $\rho$ is 1.07, it can be seen that the overall RMSE is low.

Fig. 7 (e) and (f) show the average RMSE of the tracking results according to the parameter $\rho$ for the final decision on the optimal value of $\rho$. In Fig. 7 (e), in the first scenario, when $\rho$ is 1.07 for both position and velocity, the average RMSE is the lowest at 54.69 m and 0.53 m/s, respectively, and it can be seen that other average RMSE values are higher than when $\rho$ is 1.07. In Fig. 7 (f), the second scenario, when $\rho$ is 1.07 and 1.09, the position average RMSE are 68.60 m and 70.35 m, and the velocity average RMSE are 0.76 m/s and 0.68 m/s, respectively. In the case of other $\rho$, it can be seen that the average RMSE is relatively high. From these results, it can be concluded that the optimal tracking performance when the HDCS system uses the GSFM pulse train waveform is when $\rho$ is 1.07 in the current simulation environment. The reason $\rho$ of 1.07 has the best tracking performance is that the trade-off relationship between the detection performance and measurement uncertainty is well-adjusted.

## V. CONCLUSION AND FURTHER DISCUSSIONS

### A. CONCLUSION

In this study, we propose a generalized sinusoidal frequency modulated (GSFM) pulse train waveform design considering HDCS tracking performance. The proposed design scheme utilizes the trade-off relationship between the detection performance in a reverberation environment and the measurement uncertainty according to the parameter $\rho$ of the GSFM waveform. We proposed a framework for pulse-train waveform design considering the tracking performance. In the proposed framework, the detection probability $P_D$ and measurement noise covariance matrix $\mathbf{R}$ of the Kalman filter are calculated according to the designed GSFM pulse train waveform and reflected in the tracking process. The average RMSE of the tracking results was used as the metric. In the simulation, the average RMSE was evaluated with two tracking scenarios, and it was confirmed that 1.07 is the best option for parameter $\rho$ because the trade-off relationship between the detection performance and measurement uncertainty was well adjusted at that value.

For future research, we suggest conducting the following studies: First, developing the framework that takes into account multiple clutter measurements and data association algorithm similar to a probabilistic data association filter. In addition, when evaluating the performance, it is necessary to consider various aspects, such as track initialization or track loss. Finally, it is necessary to analyze the matched filter results of the GSFM pulse train waveform for low $\rho$ using sea experimental data. This is because it is important to determine whether a sensitive trade-off relationship, such as a simulation in a real oceanic environment, is satisfied.

## APPENDIX A
## REVIEW OF TRADE-OFF RELATIONSHIP OF THE GSFM WAVEFORM

In the Sec. II-B, we claimed that the trade-off relationship of the GSFM waveform can improve the HDCS tracking performance. To evaluate whether our claim is theoretically reasonable, we analyzed the ambiguity function (AF), which assesses the measurement uncertainty, and the Q-function, which assesses the detection performance in reverberation environments [27], [30].

The AF can be expressed as follows:

$$\chi(\tau, \eta) = \sqrt{\eta} \int_{-\infty}^{\infty} s(t)\, s^*\big(\eta(t+\tau)\big) dt, \tag{35}$$

where $s(t)$ is transmitted waveform, $\tau$ is time delay, $\eta$ is Doppler scaling factor, and $*$ is conjugation. The maximum peak value of auto-AF occurs at $\tau = 0$ and $\eta = 1$, and we can analyze the range-Doppler resolution (measurement uncertainty) using the ambiguity diagram defined by the 3 dB contour of the main lobe.

The Q-function can be expressed as follows:

$$Q(\eta) = \int_{-\infty}^{\infty} |\chi(\tau, \eta)| d\tau. \tag{36}$$

Q-function is calculated under the assumption that the reverberation signal is caused by a fixed uniformly distributed and uncorrelated scatterers. Therefore, the relative difference in the Q-function level indicates a difference in the reception reverberation level for each Doppler.

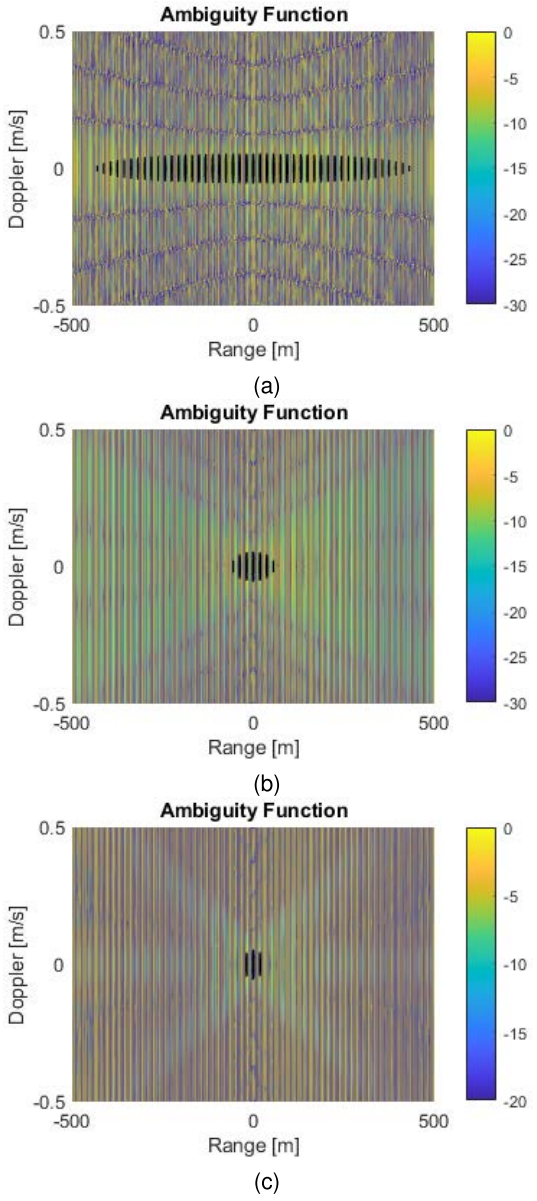


**FIGURE 8.** Comparison of ambiguity function (AF) of the GSFM waveform with $\rho$ of (a) 1.00, (b) 1.05, and (c) 1.10. The black line is the 3 dB contour of AF which means a resolution of the waveform. As $\rho$ increases, it can be seen that the range resolution is improved, but there is no significant difference in Doppler resolution.

Figs. 8 (a), (b), and (c) depict the AF of GSFM waveform with a center frequency of 3 kHz, bandwidth of 125 Hz, length of 2 s, and $C$ 80, when $\rho$ is 1.00, 1.05, and 1.10, respectively. In the figures, the range resolution (3 dB contour of AF) is narrower ( better) as $\rho$ increases and vice versa. Fig. 9 depicts the Q-function of GSFM waveform with the same specifications when $\rho$ values are 1.00, 1.05, and 1.10, respectively. In the figure, the Q-function level at Doppler value of 2.5 m/s increases (worsens) as $\rho$ increases, and vice versa. In conclusion, GSFM waveform has a trade-off relationship between measurement uncertainty and detection performance according to $\rho$.

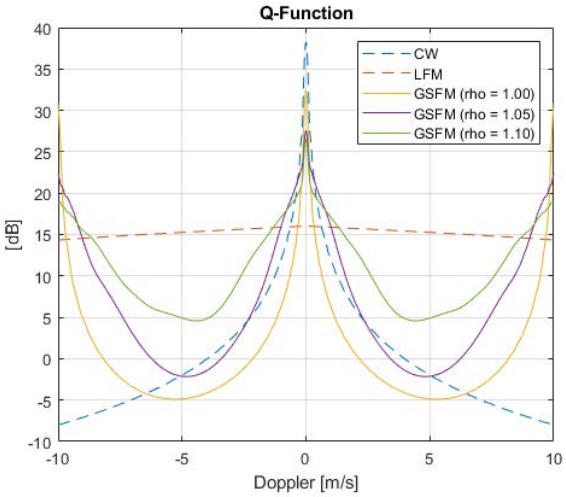


**FIGURE 9.** Analysis on the Q-function of the GSFM waveform with $\rho$ of 1.00, 1.05, and 1.10. Low value of Q-function means low reverberation power, therefore, it can be used to assess the detection performance in the reverberation environments for the target of a specific Doppler. As $\rho$ increases, it can be seen that the detection performance is decreased.

## REFERENCES

[1] R. O. Nielsen, *Sonar Signal Processing*. Norwood, MA, USA: Artech House, 1991.
[2] A. D. Waite, *Sonar for Practising Engineers*. Hoboken, NJ, USA: Wiley, 2002.
[3] R. V. Vossen, S. Beerens, and E. Spek, "Anti-submarine warfare with continuously active sonar," Sea Technology, Compass Publications, Arlington, VA, USA, 2011, pp. 33–35, vol. 52, no. 11. [Online]. Available: https://sea-technology.com/archives and https://repository.tno.nl//islandora/object/uuid:450e1df7-bccb-403a-938a-dc078d08108b
[4] S. M. Murphy, L. M. Zurk, and M. E. W. Coffin, "Processing continuous active sonar transmissions to achieve an arbitrarily fast update rate with full instantaneous bandwidth," *IEEE J. Ocean. Eng.*, vol. 46, no. 3, pp. 988–999, Jul. 2021.
[5] H. Cox, "Fundamentals of bistatic active sonar," in *Underwater Acoustic Data Processing*. Cham, Switzerland: Springer, 1989, pp. 3–24.
[6] S. Coraluppi and D. Grimmett, "Multistatic sonar tracking," *Proc. SPIE*, vol. 5096, Apr. 2003, pp. 399–410.
[7] K. Zhao, J. Liang, J. Karlsson, and J. Li, "Enhanced multistatic active sonar signal processing," *J. Acoust. Soc. Amer.*, vol. 134, no. 1, pp. 300–311, Jul. 2013.
[8] D. J. Peters, "A Bayesian method for localization by multistatic active sonar," *IEEE J. Ocean. Eng.*, vol. 42, no. 1, pp. 135–142, Jan. 2017.
[9] G. Hickman and J. L. Krolik, "Non-recurrent wideband continuous active sonar," in *Proc. Oceans*, Oct. 2012, pp. 1–6.
[10] P. C. Hines, "Experimental comparison of continuous active and pulsed active sonars in littoral waters," in *Proc. 1st Int. Conf. Exhib. Underwater Acoust.*, May 2013, pp. 51–58.
[11] D. Grimmett and C. Wakayama, "Multistatic tracking for continous active sonar using doppler-bearing measurements," in *Proc. 16th Int. Conf. Inf. Fusion*, Jul. 2013, pp. 258–265.
[12] P. C. Hines, "Experimental comparison of high duty cycle and pulsed active sonars in a littoral environment," Dept. Elect. Comput. Eng., Dalhousie Univ. Halifax (Nova Scotia), Halifax, NS, Canada, Tech. Rep., 2014. [Online]. Available: https://apps.dtic.mil/sti/citations/ADA617786
[13] R. Plate and D. Grimmett, "High duty cycle (HDC) sonar processing interval and bandwidth effects for the TREX'13 dataset," in *Proc. OCEANS Genova*, May 2015, pp. 1–10.
[14] D. A. Hague and J. R. Buck, "The generalized sinusoidal frequency modulated waveform for continuous active sonar," in *Proc. OCEANS Genova*, May 2015, pp. 1–8.
[15] C. Gianelli, L. Xu, and J. Li, "Active sonar systems in the presence of strong direct blast," in *Proc. OCEANS Genova*, May 2015, pp. 1–10.

[16] S. M. Murphy and P. C. Hines, "Sub-band processing of continuous active sonar signals in shallow water," in *Proc. OCEANS Genova*, May 2015, pp. 1–4.
[17] S. Lourey, "Adaptive filtering for enhanced detection of continuous active sonar signals," in *Proc. Underwater Acoust. Conf. Exhib. (UACE)*, 2017, pp. 145–152.
[18] K. D. LePage, G. Canepa, J. Bates, A. Tesei, M. Micheli, and A. Munafo, "Bistatic continuous active sonar processing using arrays towed from unmanned underwater vehicles," *J. Acoust. Soc. Amer.*, vol. 141, no. 5, p. 3850, May 2017.
[19] J. R. Bates, D. Grimmett, G. Canepa, and A. Tesei, "Incoherent sub-band averaging for improved target detection and Doppler estimation in linearly frequency modulated continuous active sonar," *Proc. SPIE*, vol. 33, May 2018, Art. no. 055001.
[20] J. R. Bates, S. M. Murphy, B. H. Maranda, and D. A. Abraham, "Signal-to-Reverberation ratio comparison of linear frequency modulated continuous active sonar and pulsed active sonar," *IEEE J. Ocean. Eng.*, vol. 46, no. 2, pp. 654–664, Apr. 2021.
[21] G. Kim, K. Lee, K. Yoon, and S. Lee, "A study on pulse train waveforms for high duty cycle sonar systems: Optimization scheme and relationship between orthogonality and bandwidth," *IEEE Access*, vol. 9, pp. 119800–119817, 2021.
[22] P. C. Hines, K. Hicks, S. M. Murphy, and N. Taylor, "Measurements of signal coherence for high and low duty cycle sonars in a shallow water channel," in *Proc. OCEANS Genova*, May 2015, pp. 1–5.
[23] D. Grimmett and R. Plate, "Temporal and Doppler coherence limits for the underwater acoustic channel during the LCAS'15 high duty cycle sonar experiment," in *Proc. OCEANS MTS/IEEE Monterey*, Sep. 2016, pp. 1–9.
[24] D. Grimmett, J. Itschner, D. Abraham, and L. Mazutti, "High duty cycle sonar tracking performance as a function of coherent processing interval for LCAS'15 data," in *Proc. 5th Int. Conf. Underwater Acoust.*, Jul. 2019, pp. 569–576.
[25] R. Niu, P. Willett, and Y. Bar-Shalom, "Tracking considerations in selection of radar waveform for range and range-rate measurements," *IEEE Trans. Aerosp. Electron. Syst.*, vol. 38, no. 2, pp. 467–487, Apr. 2002.
[26] Y. Sun, P. Willett, and R. Lynch, "Waveform fusion in sonar signal processing," *IEEE Trans. Aerosp. Electron. Syst.*, vol. 40, no. 2, pp. 462–477, Apr. 2004.
[27] D. A. Hague and J. R. Buck, "The generalized sinusoidal frequency-modulated waveform for active sonar," *IEEE J. Ocean. Eng.*, vol. 42, no. 1, pp. 109–123, 2016.
[28] G. Kim and S. Lee, "Reverberation suppression method for active sonar systems using non-negative matrix factorization with pre-trained frequency basis matrix," *IEEE Access*, vol. 9, pp. 148060–148075, 2021.
[29] Y. Bar-Shalom, X. R. Li, and T. Kirubarajan, *Estimation With Applications to Tracking and Navigation: Theory Algorithms and Software*. Hoboken, NJ, USA: Wiley, 2004.
[30] D. A. Abraham, *Underwater Acoustic Signal Processing: Modeling, Detection, and Estimation*. Cham, Switzerland: Springer, 2019.
[31] R. Diamant, "Closed form analysis of the normalized matched filter with a test case for detection of underwater acoustic signals," *IEEE Access*, vol. 4, pp. 8225–8235, 2016.
[32] S. M. Kay, *Fundamentals of Statistical Signal Processing: Estimation Theory*. Upper Saddle River, NJ, USA: Prentice-Hall, 1993.
[33] S. M. Kay, *Fundamentals of Statistical Signal Processing. Detection Theory*. Upper Saddle River, NJ, USA: Prentice-Hall, 1998.
[34] S. Lee and J.-S. Lim, "Reverberation suppression using non-negative matrix factorization to detect low-Doppler target with continuous wave active sonar," *EURASIP J. Adv. Signal Process.*, vol. 2019, no. 1, pp. 1–18, Dec. 2019.

**GEUNHWAN KIM** received the B.S. and M.S. degrees in electronics engineering and the Ph.D. degree in electrical and electronics engineering from Kyungpook National University, Daegu, in 2015, 2017, and 2022, respectively. Since 2022, he has been a Postdoctoral Researcher with the Department of Ocean Systems Engineering, Sejong University, Seoul, Republic of Korea. His research interests include underwater acoustic signal processing, high duty cycle sonar systems, and deep learning applications for sonar systems.

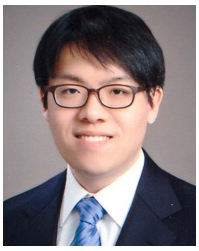

**SEOKJIN LEE** (Member, IEEE) received the B.S., M.S., and Ph.D. degrees in electrical and computer engineering from Seoul National University, in 2006, 2008, and 2012, respectively. From 2012 to 2014, he was a Senior Research Engineer at LG Electronics. From 2014 to 2018, he was an Assistant Professor at the Department of Electronics Engineering, Kyonggi University, Suwon, Republic of Korea. Since 2018, he has been an Assistant Professor (promoted to an Associate Professor, in 2020) with the School of Electrical and Electronics Engineering, Kyungpook National University, Daegu, Republic of Korea. His research interests include acoustic, sound and music signal processing, array signal processing, and blind source separation.

**KYUNGSIK YOON** received the B.S., M.S., and Ph.D. degrees in electronics engineering from Kyungpook National University, Daegu, in 1987, 1989, and 2002, respectively. From 1989 to 1995, he was a Researcher at the Agency for Defense Development. Since 1995, he has been a Professor with the College of Military ICT, Gimcheon University, Gimcheon, South Korea. His research interests include array signal processing, underwater target detection, and high duty cycle sonar.

**CHANGSOO RYU** received the B.S., M.S., and Ph.D. degrees in electronics engineering from Kyungpook National University, in 1992, 1994, and 2002, respectively. From 1994 to 1998, he was a Researcher at the Agency for Defense Development, Republic of Korea. Since 2002, he has been a Professor with the Division of ICT Semiconductor and Electronics, Yeungnam University College, Daegu, Republic of Korea. His research interests include underwater target detection and tracking, sonar signal processing, and array signal processing.

**MINSEUK PARK** received the B.S. and Ph.D. degrees in naval architecture and ocean engineering from Seoul National University, in 2010 and 2021, respectively. From 2010 to 2011, he was a Senior Staff at STX shipbuilding. He is currently an Assistant Professor with the Department of Defense Systems Engineering, Sejong University, Republic of Korea. His research interests include array signal processing, underwater source localization, and propeller cavitation.

**YOUNGMIN CHOO** (Member, IEEE) received the B.A. degree in engineering and the Ph.D. degree in underwater acoustics from Seoul National University, Republic of Korea, in 2005 and 2012, respectively. He was a Postdoctoral Research Fellow at Seoul National University and the Scripps Institution of Oceanography, from 2012 to 2016. He has been an Assistant Professor with the Department of Defense Systems Engineering of Sejong University, Republic of Korea, where he is currently an Associate Professor, since 2016. He has particular research interest in the areas of signal processing and underwater acoustics. His main research interests include scattering and reverberation from rough boundaries, sonar signal processing of beamforming, and ocean parameter inversion from data.